Deformation behavior and dislocation structure of CuAu ordered alloy

O.V. Antonova, B.A. Greenberg, A.Yu. Volkov

Institute of Metal Physics, Ural Branch, Russian Academy of Sciences,
18 S. Kovalevskaya St., Ekaterinburg 620041, Russia

Abstract

An ordered CuAu alloy, which had relatively coarse grains (5 to 10 μm), without the lamellar structure, is mechanically tested at temperatures from 77 to 658 K. The temperature dependence of the yield stress is shown to be anomalous with a maximum near T_p≈573 K. The TEM analysis reveals the presence of single dislocations, superdislocations and microtwins. Long rectilinear dislocations at 523 K are identified as blocked screw superdislocations with the Burgers vector type <101]. Numerous curved single dislocations are seen, but blocked single dislocations are not detected. Various models are discussed to account for the specific deformation behavior of the ordered CuAu alloy.

Keywords: Ordered alloys and intermetallics, dislocation transformations, thermal anomaly of the yield stress, a copper-gold alloy.

Introduction

The equiatomic CuAu alloy (the $L1_0$ superstructure) is the basis of jewelry, dental and electrotechnical materials and for this reason it has been studied in sufficient detail [1-4]. It was found that the atomic ordering in this alloy is accompanied by the formation of a stable lamellar structure comprising *c*-domains of different orientations. For this reason, virtually all the studies are devoted to the dependence of the alloy properties on the size of the lamellae. Small dimensions of the lamellae hampered a detailed study of the dislocation structure of the ordered CuAu alloy and, therefore, the focus has been on processes of the dislocation rearrangement at domain boundaries [4, 5].

Recently the interest to the dislocation structure of ordered alloys and intermetallics has considerably increased because of the discovery of the temperature anomaly of the yield stress in some alloys with a long-range atomic order. It has been assumed to be an established fact that this temperature anomaly is due to blocking of dislocations. For example, the temperature peak of the yield stress in a single crystal of TiAl is accompanied by the evolution of superdislocations of the two types and single dislocations, which are blocked via their specific thermally activated mechanisms in this material [6].

It is interesting to determine the temperature dependence of the yield stress of the CuAu alloy having the same $L1_0$ type of the superstructure as TiAl has. It is worth seeing whether the temperature anomaly of the yield stress takes place and blocked dislocations are observed in this alloy.

It is known that the temperature anomaly of the yield stress is observed only in coarse-grain materials. The critical size of grains, below which the $\sigma_{0.2}(T)$ anomaly is not observed, is different in different alloys: ≈ 8 μm in Ni_3Al and ≈ 50 μm in TiAl [7]. However, to the best of our knowledge, all attempts to make an ordered single crystal of CuAu have failed.

A plateau on the temperature dependence of the yield stress was revealed in wire samples of the ordered CuAu alloy at temperatures between 77 and 373 K in [4]. The alloy in this work had grains nearly 1.0 μm in size and contained domain boundaries. Obviously, determining the possibility of the thermal strengthening and a detailed study of dislocation transformations in the ordered CuAu alloy requires samples having still coarser grains and a minimum number of domain grains.

We studied the evolution of the microstructure in the CuAu alloy during its ordering [8-10]. It was revealed that the microstructure and the domain size can be considerably affected by varying the conditions used for thermal treatment of the alloy. Our method providing an ordered structure in the CuAu alloy with grains-monodomains about 10 μm in size is described in [9]. The alloy virtually did not contain domain boundaries.

This work deals with processes of the plastic deformation in the CuAu alloy, which is free from domain boundaries, at

temperatures between 77 and 658 K by mechanical tests and electron-microscopic examination.

Materials and methods

A stoichiometric CuAu alloy was prepared from 99.99% metals by vacuum-melting and then was subjected to a thermomechanical trearment. After homogenization at 1123 K for 3 h and subsequent quenching in ice-cold water, the disordered alloy was rolled to 65% reduction. The sample was rapidly heated to 668 K and was allowed to stay at this temperature for 12 h. Subsequently it was cooled at the rate of 10°/day. Under these treatment conditions, the CuAuII alloy recrystallized and the CuAuII phase transformed into CuAuI when the temperature was reduced. As a result, we obtained a polycrystal of the ordered CuAuI alloy, which was almost free of the lamellar structure, i.e., colonies of *c*-domains, and had relatively coarse grains nearly 10 μm in size.

Tensile test samples were cut out of 0.1 mm thick alloy plates. The test portion of the samples was 30 mm long and 3.2 mm wide. The mechanical tests were performed over the temperature interval from 77 to 658 K. The temperature was measured to within ± 2 K. The alloy samples were held at the assigned temperature for 20 min prior to deformation. The structure was analyzed using a JEM-200CX electron microscope. Foils were prepared using a standard technique from samples deformed to 3% and from failed samples.

When studying the dislocation structure, the Burgers vectors were determined using the **gb** analysis in the reflections **g** listed in Table 1. A special program was used to calculate the axis of dislocation from its projections in three sections of the reciprocal lattice.

Figure 1

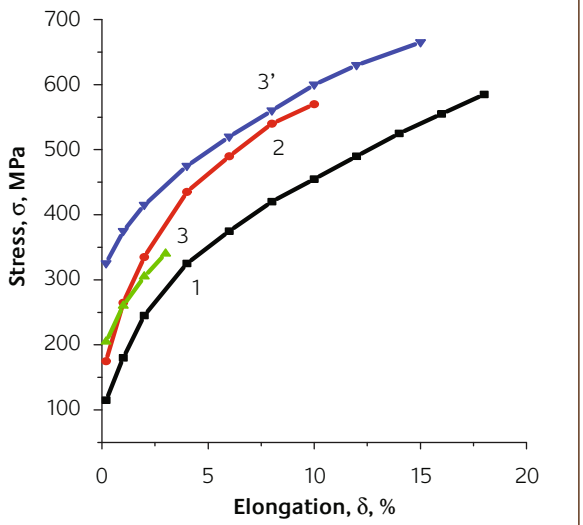

Tensile diagrams of the coarse-grained ordered CuAu alloy at different test temperatures:
1 – 293 K;
2 – 77 K;
3 – 573 K;
3' – additional test at room temperature subsequent to deformation at 573 K

Results

Mechanical properties

Fig.1 shows tensile curves for the CuAu alloy with such coarse-grained structure tested at 77, 293 and 573 K (curves 1, 2 and 3). Curve 3´ corresponds to a second step of deformation, which was realized at room temperature after the first step of deformation at 573 K (curve 3). These diagrams display the effect of the temperature on the

Table 1

*Values of **gb** for various dislocations*

b	g										
	020	200	111	$\bar{1}11$	110,$\bar{2}20$	110, 220	$3\bar{1}\bar{1}$	021	311	131	$3\bar{1}1$
1/2a[110]	1	1	1	0	0	1	1	1	2	2	$\bar{1}$
1/2a[$\bar{1}$10]	1	$\bar{1}$	0	1	1	0	2	1	1	1	$\bar{2}$
a[101]	0	2	2	0	$\bar{1}$	1	2	1	4	2	4
a[$\bar{1}$01]	0	$\bar{2}$	0	2	1	$\bar{1}$	$\bar{4}$	$\bar{1}$	$\bar{2}$	0	$\bar{2}$
a[011]	2	0	2	2	1	1	2	3	2	4	0
a[0$\bar{1}$1]	$\bar{2}$	0	0	0	$\bar{1}$	$\bar{1}$	0	$\bar{1}$	0	2	2
1/2a[112]	1	1	2	1	0	1	0	2	3	3	2
1/2a[$\bar{1}$12]	1	$\bar{1}$	1	2	1	0	$\bar{2}$	2	0	2	$\bar{1}$
1/2a[1$\bar{1}$2]	$\bar{1}$	1	1	0	$\bar{1}$	0	2	0	2	0	3
1/2a[11$\bar{2}$]	1	1	0	$\bar{1}$	0	1	2	0	1	1	0

Figure 2

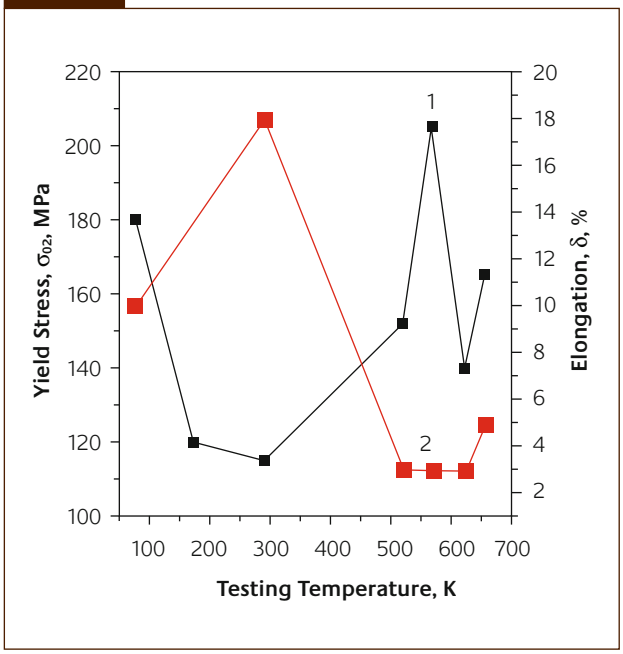

Temperature dependences of the yield stress $\sigma_{0.2}$ (curve 1) and the elongation δ (curve 2) of the ordered CuAu alloy with coarse-grained structure

deformation behavior of the alloy, primarily, the loss of plasticity and the rise of strength at temperatures differing from room temperature.

Fig.2 shows the yield stress $\sigma_{0.2}$ and the elongation δ as a function of the test temperature. Both quantities exhibit a non-monotonic temperature trend. From curve 1 in Fig.2 it is seen that $\sigma_{0.2}(T)$ has a maximum near $T_p \approx 573$ K. The $\sigma_{0.2}$ value at T_p is nearly twice as high as the value at room temperature. A sharp drop of the elongation from 18% at room temperature to 3% at 523 K is particularly significant (curve 2 in Fig.2). The plateau observed in the $\delta(T)$ curve and the peak observed in the $\sigma_{0.2}(T)$ curve at temperatures between 523 and 623 K suggest that the temperature dependences of these characteristics are controlled by different mechanisms.

Microstructure

Typical fields of the microstructure of the coarse-grained CuAu alloy, deformed at different temperatures, are reproduced in Fig.3-6. The electron-microscopic examination of the samples deformed to 3% at all the test temperatures showed that deformation in the material occurs by both the slip of dislocations (both single and superstructural) and the twinning. No substantial changes in microstructure were observed after the tests at temperatures between 77 and 573 K. The observations only show, to the accuracy which electron microscopy permits, that the twinning is somewhat suppressed at room temperature. Therefore, the microstructure examination was focused mainly on the dislocation structure.

Figure 3a, b, c

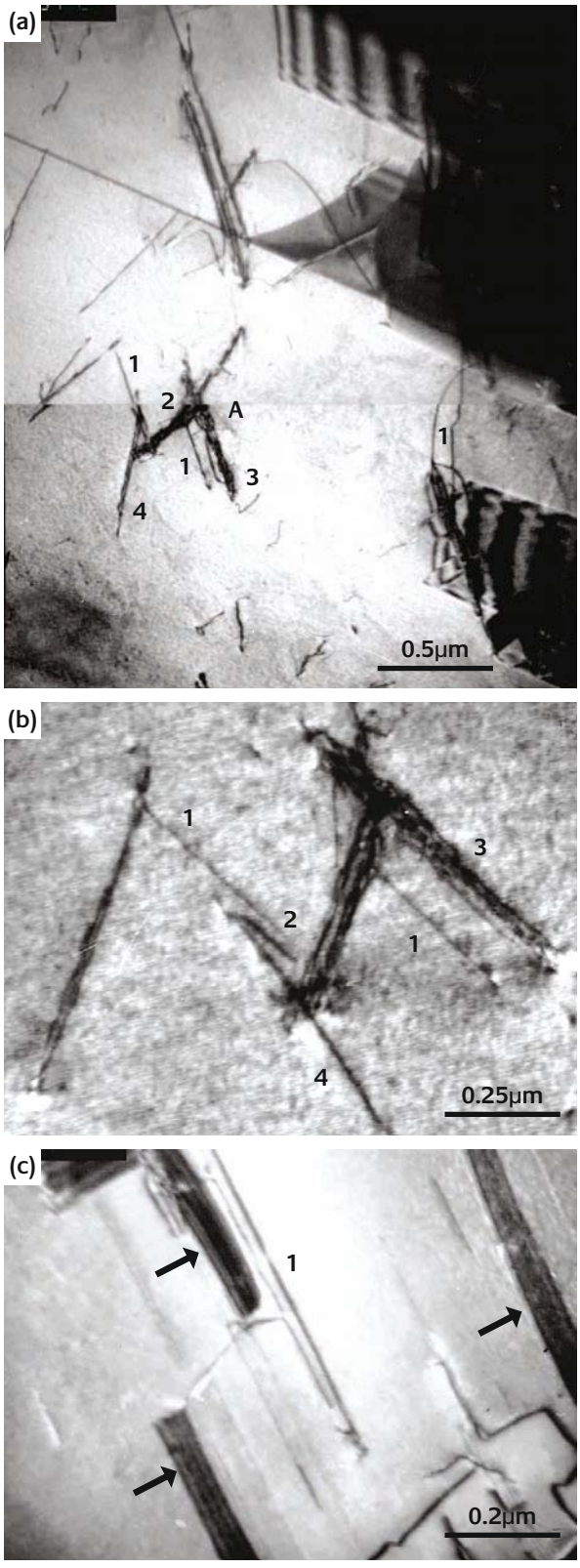

Microstructure of the CuAu alloy deformed by 3% at 77K :
a) bright-field image of the dislocations and stacking-fault twins;
*b) dark-field image of dislocation configuration **A** in **g**= [111], **BD** [11$\bar{2}$];*
*c) dark-field image of the superdislocation a[101] b **g**=[110], **BD**[3$\bar{3}$2]; the arrows indicate APBs*

Figure 3d, e, f, g

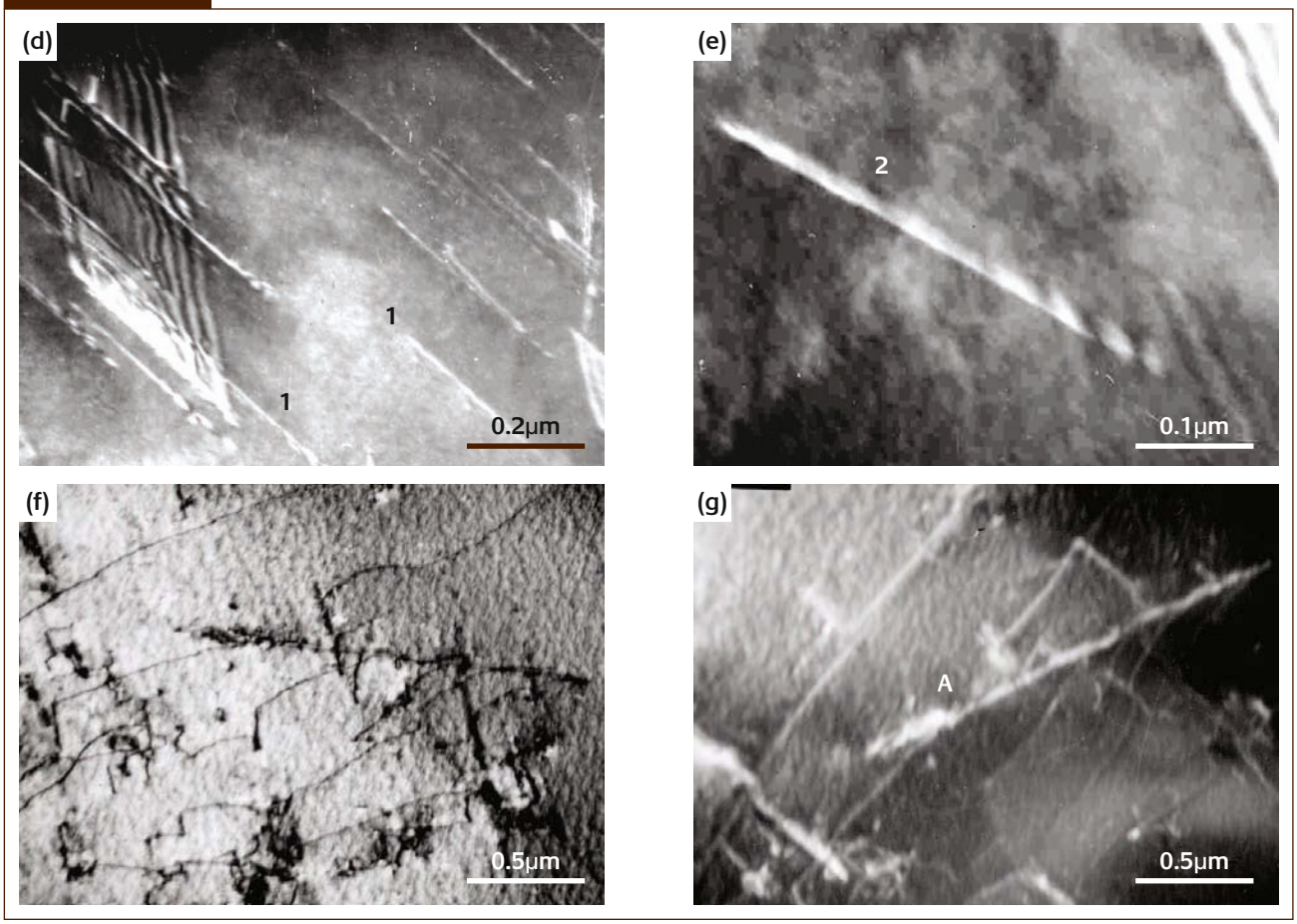

Microstructure of the CuAu alloy deformed by 3% at 77 K:
d, e) microstructure of the [101] grain, dark-field image in ***g****=[11$\bar{3}$];* ***BD*** *[314];*
f) bright-field image of a grain with a high density of single dislocations;
g) dark-field image in ***g****=[11$\bar{3}$],* ***BD*** *[211]*

Deformation at 77 K

Fig.3 presents a typical microstructure fragment of a grain in which the deformation was accomplished mainly by the dislocation slip. Using different diffraction conditions, we reveal that both single dislocations and superdislocations are present in the configuration **A** shown in Fig.3a. For example, dislocations *1* (Figs.3a and 3b) were identified as single dislocations with the Burgers vector b = 1/2a[110], i.e., these are 60° dislocations and the slip plane is (111).

The microstructure of this grain is characterized by complex dislocation pileups labeled 2 and 3 that have a certain crystallographic orientation. We unambiguously determined only their preferred orientations ([101] and [011] for configurations 2 and 3, respectively). Their internal structure, which is most clearly seen in the dark-field images taken in the [020] and [111] reflections (Fig.3b), consists of parallel dislocation lines with jogs and constrictions. For example, the image taken in the [111] reflection displays three lines for configuration 3. The spacings between them are about 7-12 nm. This order of magnitude suggests that, in this case, we see split dislocations. Based on the results of the determination of dislocation emergence onto the foil surface, we rule out that they are dipoles. According to the diffraction conditions used, the width of dislocation configuration 3 should not alter with changing the foil inclination. However, in the reflection **g** = [3$\bar{1}$ $\bar{1}$], we saw the so-called residual contrast. This result can be realized for perfect dislocations with **b** = 1/2a[112] and **b** = a[0$\bar{1}$]. The latter dislocation was excluded from the consideration because it was not extinguished in other reflections appropriate for its extinction. Thus, we can assume that the dislocation with **b** = 1/2a[112] is dissociated according to the reaction established in [6] for TiAl:

1/2<112] → 1/6[2$\bar{1}$1] + CSF + 1/6[112] + APB + 1/6[$\bar{1}$21] + SISF + 1/6[112], (1)

1/2<112] → 1/6[112] + SESF + 1/3[112], (2)

1/2<112] →1/2[011] + APB + 1/6[2$\bar{1}$1] + SISF + 1/6[112], (3)

where CSF is a complex stacking fault consisting of an antiphase boundary (APB) and a superstructural intrinsic or extrinsic stacking fault (SISF or SESF, respectively).

The reactions are complanar, and the conditions of the extinction in the **g** = [3$\bar{1}\bar{1}$] reflection are fulfilled only for Eq.(2). This type of dissociated dislocations are characterized by the least mobility, since the intrinsic stacking faults are

bounded by partial Shockley dislocations. We should add that in the reflection **g** = [1$\bar{1}$0] we observed a partial disappearance of the contrast and observed no contrast typical of antiphase boundaries (APB). This result is likely to require additional research in order to confirm the dissociation of superstructural dislocations 1/2a<112], the more so that no superdislocations with such a vector were found in a free form.

Dislocation *4* is seen as two lines and its emergences to the surface have the same intensity (Fig.3a). Therefore it was indexed as a paired superdislocation with total **b** = a[011]. In the [020] reflection, the dislocations exhibit an oscillating contrast typical of condition **gb** = 1/2[011] • [020] = 1. The dislocation axis calculated from the projections in tree sections of the reciprocal lattice is close to the direction u_4 = [110].

The deformation in this grain also occurred by the propagation of twinned stacking faults generated at the grain boundary. The defect plane was determined to be (11$\bar{1}$) from parameters such as the foil plane (11$\bar{2}$), the emergence points of the defect onto the foil plane, the [$\bar{1}\bar{1}$0] orientation of the stacking-fault intersection with the foil plane, and the angle of 20.4° between the stacking fault and the foil surface. The full extinction of the contrast both from defects and from the twinning dislocations was obtained in the reflections **g** = [2$\bar{2}$0] and **g** = [3$\bar{1}\bar{1}$], corresponding to the shear **R** = 1/6a[112]. This result is confirmed by the contrast at the twinning dislocations in the [202] and [022] reflections, satisfying the condition **gb** = 1. These dislocations react with single dislocations *1*, forming Frank sessile dislocations,

$$1/2[\bar{1}\bar{1}0]_{(\bar{1}11)} + 1/6[112]_{(11\bar{1})} = 1/3[1\bar{1}\bar{1}], \quad (4)$$

which act as barriers to a further propagation of stacking faults (Fig.3a).

Note that the cubic slip of superdislocations of the a/2<101] type with long antiphase boundaries between them is observed in the CuAu alloy both at cryogenic and elevated temperatures. Such antiphase boundaries present in the (010) plane are seen in the microstructure of a grain with the [3$\bar{1}$4] orientation (Fig.3c). It was established that virtually all rectilinear dislocations are superdislocations. The screw superdislocation *1* is characterized by b = a[$\bar{1}$01].

Many rectilinear dislocations are exhibited in the grain with orientation [101] (Fig.3d, e). In this case all dislocations were found to be superdislocations which have the direction [10$\bar{1}$]. It was established that dislocations *1* and *2* have the total Burgers vector a/2[$\bar{1}$12]. The dislocations are of the 30° type, and its slip plane is (1$\bar{1}$1). Fig. 3e presents a dark-field image of the 1/2[$\bar{1}$12] superdislocation with different intensities of the dislocation lines and the fringe contrast typical of stacking faults between them. These features show that the dislocations are dissociated. The dislocation image in the [20$\bar{2}$] reflection was separated into three lines with the spacing of ≈ 6 nm between them. In this work, we failed to unambiguously determine the Burgers vector of the superpartial dislocations, but the existing data on the dissociation of <112] dislocations in TiAl and the presence of SISF in the CuAu microstructure suggest the following reaction:

$$1/2[\bar{1}12] = 1/6[\bar{1}12] + \text{SISF} + 1/3[\bar{1}12]. \quad (5)$$

The dissociation of these dislocations is indirectly confirmed by the presence in the grain of stacking faults lying in the (1$\bar{1}$1) plane and characterized by the [$\bar{1}$12] shear vector. Such twinning stacking faults have already been observed in CuAu after room-temperature deformation in [4]. Their formation was explained by the action of a pole mechanism on the basis of dissociated superdislocations. In this work, we observed a pileup of superdislocations with **b** = a/2[$\bar{1}$12] in the nearest proximity to the stacking fault. In this grain, we also observed screw superdislocations with **b** = a[$\bar{1}$01]. Since the alloy was deformed by tension, we failed to exactly determine the loading direction.

Figures 3f and 3g present the microstructure of a grain with the orientation [231]. The deformation in this grain is realized mainly by single dislocations. Their Burgers vectors were determined to be **b** = 1/2a[1$\bar{1}$0]. Some of these dislocations underwent interaction with the rectilinear superdislocation (**A**) with the [01$\bar{1}$] orientation, forming a complex dislocation configuration. The presence of a contrast at this dislocation allows us to exclude the single dislocations and superdislocations with the Burgers vectors a<101>, a[011], and 1/2<112]. Some dislocation fragments were observed to be extinguished in the reflection **g** = [$\bar{1}$11], and a diffuse contrast ≈ 10 nm wide was observed in the [$\bar{1}\bar{1}$3] reflection (Fig.3g). This is likely to be caused by the dissociation of the dislocation with a total vector equal to either a[011] or 1/2a[1$\bar{1}$2]. These are dislocations of screw and mixed types, respectively; they can interact with surrounding single dislocations b = 1/2a[1$\bar{1}$0], and, depending on the type of the dissociation of the superstructural dislocation and the slip plane of the single dislocations, form blocked or glissile configurations [4].

Deformation at room temperature

Room-temperature deformation of the alloy occurs by the slip of all types of dislocations and by the twinning. Fig. 4a shows a microstructure typical of this state. A grain with the orientation close to [21$\bar{2}$] has a relatively high density of rectilinear single dislocations (shown by arrows). The presence of large kinks in these single dislocations is quite remarkable. Most dislocations in Fig. 4a have been identified as single dislocations with the Burgers vector 1/2[1$\bar{1}$0] since they are invisible with **g** = [111] (see Fig.4b) and **g** = [001].

In addition to single dislocations, the grain microstructure in Fig. 4a contains twinned stacking faults, a dislocation configuration designated as **A**, and short curved dislocation segments adjacent to these elements (see Fig. 4c). It was determined that the twinned stacking faults lie in the ($\bar{1}$11) plane and have the shear vector **R** = 1/6a[1$\bar{1}$2] and that the adjacent dislocations are single dislocations with the Burgers vectors **b** = 1/2a[1$\bar{1}$0]. The interaction of these dislocations

Figure 4

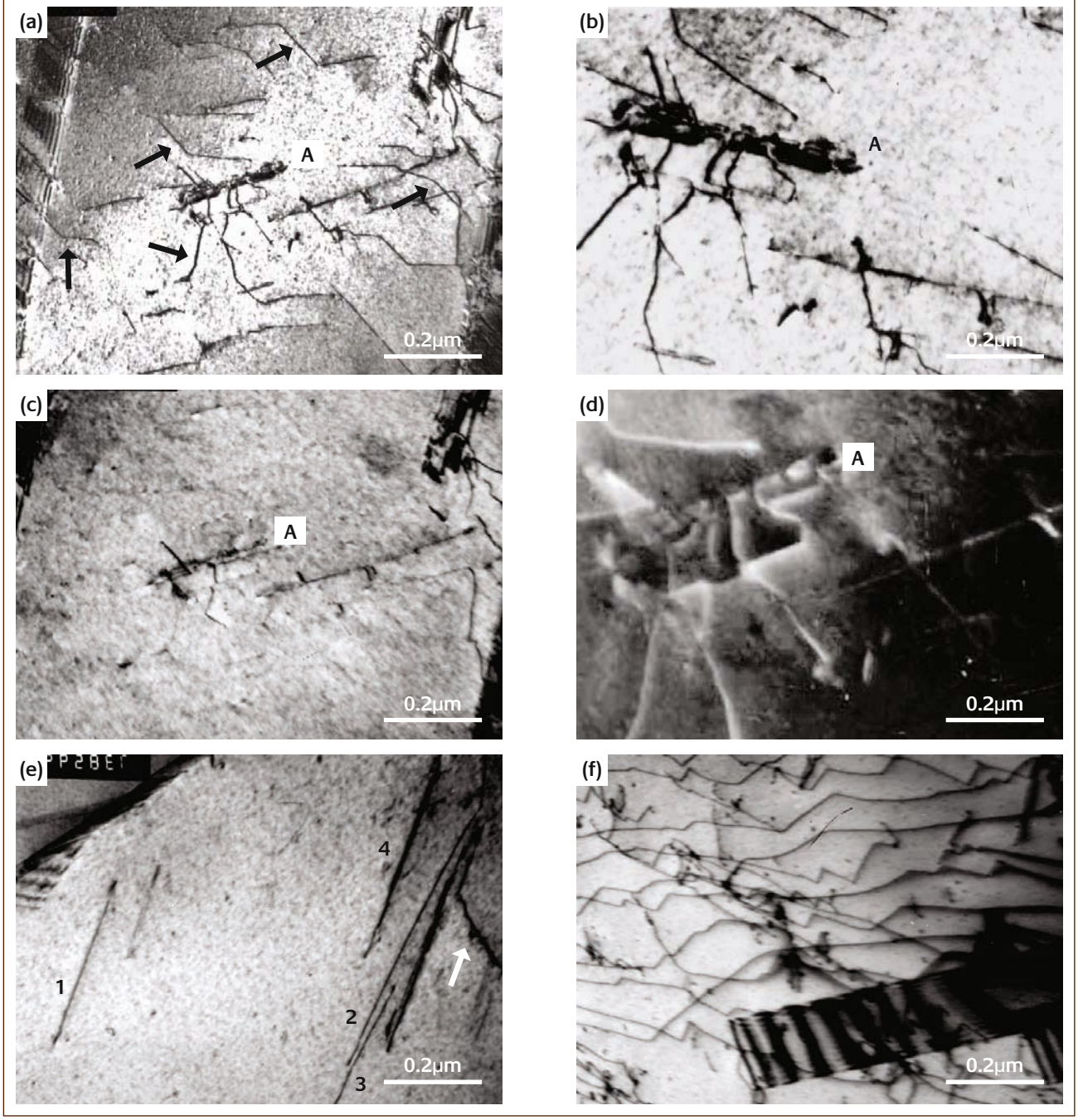

Microstructure of the CuAu alloy deformed by 3% at room temperature: a) bright-field image (the arrows indicate single dislocations); b) dark-field image in ***g****=[020],* ***BD*** *[10$\bar{1}$] of the dislocation configuration A; c) dark-field image in* ***g****=[111],* ***BD*** *[10$\bar{1}$]; d) dark-field image of region A in* ***g****=[1$\bar{3}$1],* ***BD*** *[10$\bar{1}$]; e) bright-field image of the area with superstructural dislocations; f) bright-field image of single dislocations and a stacking-fault twin*

with twinning dislocations causes the formation of a Frank sessile dislocation and thus hinders the twin propagation.

An analysis of the contrast in various reflections showed that the internal structure of the dislocation configuration **A**, whose crystallographic orientation was calculated to be close to [011], is of a complex character. The image taken in the **g** = [111] reflection contains rectilinear dislocations and extinguished single dislocations that have reacted with the rectilinear ones. In the [1$\bar{1}$0] and [$\bar{1}$3$\bar{1}$] reflections (Fig. 4d), rectilinear segments oriented in the [011] direction become extinguished. This is possible for dislocations with the Burgers vector **b** = 1/2a[112]. The diffuse contrast in **g** = [$\bar{1}$11] points to the presence of stacking faults.

The 1/2a<112] superstructural dislocations were also observed in the microstructure in the free form. In Fig. 4e, dislocations *1-4* are superdislocations, since they have good contrast in the reflection **g** = [002]. We unambiguously established the Burgers vector of dislocations *1-3* to be

b = a[$\bar{1}$01]. The contrast at dislocation *4* was observed in the reflection **g** = [$\bar{1}$10] and was absent in the reflection **g** = [0$\bar{1}$1]. This suggests that the Burgers vector of this dislocation is $\mathbf{b}_4$ = 1/2a[$\bar{1}$12]. The axes of dislocations *1* and *4* were calculated to unambiguously be [$\bar{1}$01]. Then, dislocation *1* is of the screw type and dislocation *4* is 30°, and they lie in the (111) and ($\bar{1}1\bar{1}$) planes, respectively. In the region indicated by arrow at Fig.4e, the dislocations are single and have b = 1/2a[110].

Note that at room temperature the role of single dislocations in deformation processes is enhanced. In some grains they constitute the major part of the dislocation density (Fig. 4f).

Deformation at 523 K

In this case the microstructure is generally characterized by a long rectilinear dislocation. Figs. 5a,b show type <101] superdislocations whose parameters were established exactly. The Burgers vector of dislocation *1* was determined to be $\mathbf{b}_1$ = a[101] and the axis orientation is [101], i.e. the dislocation is

Figure 5

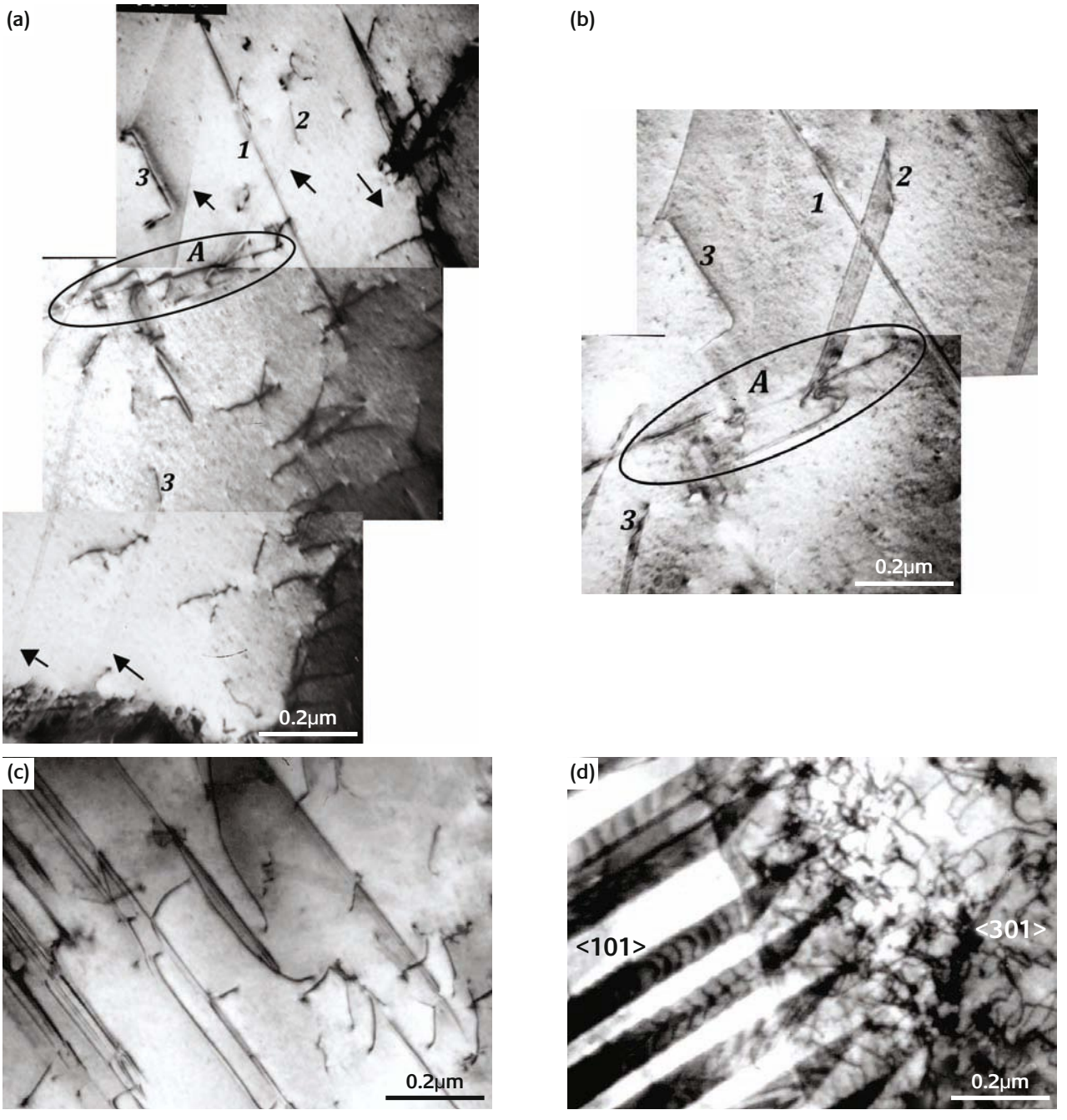

Microstructure of the ordered CuAu alloy deformed at 523 K: a) bright-field image (the arrows indicate APBs); b) dark-field image of the microstructure fragment in ***g*** *= [200],* ***BD*** *[01$\bar{1}$]; c) bright-field image of blocked screw dislocations with* ***b*** *= a[011]; d) bright-field image the boundary of two grains*

of the screw type. The double contrast observed in some reflections suggests that this dislocation is dissociated. We failed to exactly establish the type of its extension at the electron-microscopic resolution used, but it is noteworthy that we observed a diffuse contrast of about 20 nm wide in the image plane close to (010) upon extinction in **g** = [20$\bar{2}$]. We attributed this contrast to stacking faults. The spacing between the partial dislocations in the image plane ($\bar{3}$55) deviating from ($\bar{1}$11) by 15° is about 13 nm. These data are consistent with the width of the Kear-Wilsdorf (K-W) barrier for TiAl and Ni_3Al alloy [11, 12]. Therefore, we assume that dislocation *1* is blocked by the K-W mechanism.

The dislocation configuration **A** consists of a superstructural dislocation of the screw type: its total Burgers vector is **b** = a[$\bar{1}$01]. As is seen from Figs. 5a and 5b, this dislocation is separated into fragments consisting of single dislocations and partial superstructural dislocations. The Burgers vectors of these single dislocations were determined to be b = 1/2a[$\bar{1}$10] and b = 1/2a[110]. As a rule, after testing at 523 K the single dislocations are presented by short curved segments, which form pileups. In Fig. 5a they are shown as short curvilinear segments (see the right side of the figure).

Superdislocations 2 in Figs. 5a and 5b were identified as having the Burgers vector $\mathbf{b}_2$ = 1/2a[011] from the extinctions in the [200], [11$\bar{1}$], and [02$\bar{2}$] reflections. These dislocations, corresponding to the same result of the **gb** analysis, are joined by an APB. The APB extension between the dislocations is ≈ 440 nm. The dislocation axis was calculated to have the [032] orientation, i.e., the dislocation is close to the screw orientation (ϕ = 11°), and its slip plane is (100).

Note that the density of superdislocations with extended APBs is rather high. These dislocations are emitted by either the grain boundary located in the lower portion of the micrograph or (similarly to dislocations 2) by a source present inside the grain. As was shown by the **gb** analysis, dislocation 3 has the Burgers vector $\mathbf{b}_3$ = 1/2a[01$\bar{1}$], which was determined from the absence of the contrast in **g** = [111] and [200]. The dislocation axis is parallel to [0$\bar{1}$3], the orientation is close to 30°, and the dislocation slip occurs in the (100) plane. In this case, the width of the APB following the superpartial is ≈1500 nm. This indicates the activation of the slip of superdislocations in the cube plane upon room-temperature deformation. Blocked single dislocations are not observed.

Blocking of superdislocations in the CuAu alloy at this deformation temperature is illustrated additionally in Fig. 5c where we can see a series of rectilinear dislocations, which were identified as screw dislocations with **b** = a[01$\bar{1}$]. A double contrast ≈8 nm wide in the (100) image plane is formed on these dislocations under some diffraction conditions. The double contrast decreases a little in the (111) plane, and is about 10 nm wide in the (2$\bar{1}$1) plane (deviating from the (1$\bar{1}$1) plane by 19°). Based on these results, we assume that we are dealing with K-W barriers.

In addition to the dislocation mode, the twinning was also responsible for plastic deformation of the CuAu polycrystal. Twins were observed over the entire temperature interval studied. Boundaries of two grains are shown in Fig. 5d. Deformation of the grain with the <101> orientation was due mainly to the twinning. A system of parallel microtwins stopped by the grain boundary can be seen. Deformation of the other grain was realized by the dislocation slip.

Discussion

It is known that the yield stress of fcc metals weakly depends on the temperature. As follows from [13], the formation of a superlattice affects little this dependence except when ordered systems exhibit an anomalous deformation behavior such as a positive $\sigma_{0.2}(T)$ dependence. It is exactly such a nonmonotonic temperature dependence of the yield stress that was found for the CuAu alloy (Fig. 2).

Comparing the obtained results with the data for TiAl ($L1_0$), we can note the following: the TiAl superstructure is formed directly from the melt, whereas the temperature range of the $L1_0$ superstructure in the CuAu alloy is substantially smaller and lies below 410°C. Therefore, it is reasonable to consider the degree of long-range ordering as a function of the temperature. The review of the literature on the yield stress as a function of the degree of ordering shows that for most ordered structures the strengthening factor considerably increases at the degree of ordering S = 0.5-0.7 because of the altered mobility of superdislocations. In the CuAu alloy the degree of ordering decreases from 1 to 0.8 as the order-disorder transition temperature is approached [4]. This effect was explained by the modulated interaction of moving dislocations with local disordered regions formed in the domain structure upon heating.

The decrease in the degree of ordering in the CuAu alloy at temperatures below the point corresponding to the maximum ordering rate (300-350°C) is as small as a few hundredths and does not exceed 0.1 [4, 14]. In our opinion, this should not substantially affect the yield stress of the CuAu alloy without domain boundaries at temperatures up to 350°C. Therefore, the observed maximum in the $\sigma_{0.2}(T)$ curve is caused most likely by the specific structure evolution at increasing temperature, in particular, by the specific dislocation structure observed, e.g., in TiAl ($L1_0$) [6, 12].

Notice that the realization of plastic deformation over a wide temperature interval by the simultaneous action of two mechanisms such as the twinning and the dislocation slip is unusual for fcc materials. This fact was first observed in [15], where the structure of the CuAu alloy under room-temperature plastic deformation was studied. According to Pashley *et al.* [16], the dominating room-temperature deformation mode in CuAu is {111}<112] twinning, which does not break the symmetry of the $L1_0$ lattice. The main attention in these works was paid to the interaction of dislocations and twin defects with domain boundaries filling the grains.

The mechanical twinning in alloys with a low stacking-fault energy (SFE) can occur even at temperatures far below room temperature. For example, the twinning in copper and gold was observed at 4.2 K and below 77 K, respectively. With increasing temperature, deformation by the slip substitutes for the twinning and becomes dominant in most materials. It was also assumed that in ordered systems the long-range ordering hinders the mechanical twinning. There are experimental data both confirming this opinion and showing that the twinning is an active deformation mode even at elevated temperatures [17]. Microtwins in TiAl alloys with the $L1_0$ superstructure were observed after deformation to several percent at temperatures up to 400°C.

Until now it has not been clear whether or not the twinning deformation begins under some critical stress. For example, it was reported [18] that the yield stress of a Al_3Ti single crystal is independent of the temperature when deformation occurs only by the twinning. The formation of twins is conventionally believed to be caused mainly by the presence of concentrators of elastic stresses in crystals. According to our results, twinning dislocations in the CuAu alloy are generally emitted by grain-boundary dislocations.

Based on all these data, we assume that the positive dependence $\sigma_{0.2}(T)$ is not caused by the twinning. On the other hand, an intense twinning can cause brittle fracture of materials. Cracks usually begin at the grain boundary and then propagate along the twin boundaries. However, the CuAu embrittlement observed at high test temperatures cannot be explained only by the twinning, since a rather high plasticity was observed at room temperature when the twinning deformation mode is active too. Therefore, the role of the twinning in alloys with the $L1_0$ superstructure requires a special study.

The abrupt decrease in the plasticity of ordered alloys containing impurities was reported in many works. In our experiments the plastic deformation behavior was not different in samples with different grain sizes. The detrimental effect of impurities can also be excluded based on the results of two-step tests. When segregates of small impurities are formed at grain boundaries during deformation at elevated temperatures, they should be retained after cooling to room temperature and cause a low plasticity. However, when we returned to room-temperature tests, we again observed a good plasticity of the alloy (Fig.1, curve 3').

Thus, the nonmonotonic temperature dependence of the yield stress is caused most likely by dislocation processes resulting in dislocation blocking similar to that observed earlier for TiAl. In reality, TEM studies revealed both the similarity of the deformation modes in these two alloys and some differences. No blocked single dislocations typical of TiAl [6] were observed in the ordered CuAu alloy over the entire temperature range used. This type of the dislocation blocking in TiAl is related to the multi-valley Peierls relief, which is absent in CuAu. Therefore, we can expect that no anomalous yield stress behavior would be observed for the CuAu single crystal at the orientation favorable for the slip of single dislocations.

Figure 6

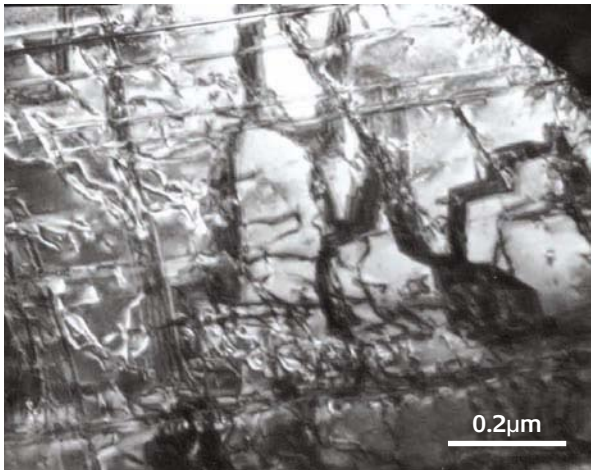

Microstructure of the ordered CuAu alloy after deformation at 623 K

From the viewpoint of the blocking of superdislocations, the dislocation configuration consisting of a rectilinear superdislocation and wavy segments of single dislocations emitting from it (configuration **A** in Fig. 4a-d) is of particular interest. Such dislocation configurations observed in the TiAl intermetallic at 400°C were called "dendrites" [6]. Their formation is caused by the initial blocking of a<101> superdislocations and the subsequent capture of single dislocations.

The fact that in the sample tested at 523 K we observed rectilinear screw a<101> dislocations producing a double contrast at the resolution used is consistent with the observed positive temperature dependence of the yield stress in this temperature range. The anomaly of $\sigma_{0.2}(T)$ in TiAl was attributed to the observed blocking of superdislocations through the K-W mechanism [12]. The whole body of the obtained data shows that the positive temperature dependence of the yield stress in the ordered CuAu alloy is also caused by the action of the Kear-Wilsdorf mechanism.

We explain the decrease in the yield stress at 623 K by the active role of the cubic slip. Fig. 6 presents a high density of APBs, which are present mainly in cube planes and terminate at dislocations. The subsequent increase in $\sigma_{0.2}(T)$ at 658 K could be due to the formation of the long-period CuAuII structure that was observed at this temperature in [9]. This structure is known to surpass CuAuI in strength properties [4].

Conclusion

The ordered CuAu alloy is characterized by a nonmonotonic temperature dependence of the yield stress, which is minimum at room temperature and maximum at 573 K.

Deformation is realized by the twinning and the slip of both single dislocations and superdislocations. The maximum observed at 573 K is explained by the blocking of screw a<101> superdislocations through the Kear-Wilsdorf mechanism. Blocked single dislocations were not detected in CuAu. Therefore, one should expect that at a favorable orientation of CuAu single crystals, unlike in TiAl single crystals, no anomaly of the temperature dependence of the yield stress will be observed.

Above room temperature the cubic slip of a<101> superdislocations, which are represented by superpartial dislocations with extended antiphase boundaries between them, makes a substantial contribution to the deformation.

Acknowledgements

This work was supported from the state budget on the topic "Structure" (No. 01.2.006 13392) and by the Russian Fundamental Research Foundation (Grants No. 07-03-00144 and No. 08-03-99046) and the Russian Science Support Foundation.

About the authors

Dr. O.V. Antonova is a Senior Researcher at the Institute of Metal Physics, Ural Branch RAS. She is a specialist in electron microscopy and investigates the dislocation structure, microstructure and phase transformations of ordered metals and intermetallics.

Prof. B.A. Greenberg is a Professor and Head of Laboratory at the Institute of Metal Physics, Ural Branch RAS. Her scientific interests focus on a wide scope of problems in materials science, including phase transformations and the theory of strength.

Dr. A.Yu. Volkov is a Leading Researcher at the Institute of Metal Physics, Ural Branch RAS. He studies microstructure, phase transformations, physical and mechanical properties of ordered alloys based on gold and noble metals.

References

1 M. Hirabayashi, S. Weissman, *Acta Met.*, 1962, **10**, 25
2 V.S. Arunachalam and R.W. Cahn, *J.Mat.Science*, 1967, **2**, 160
3 G.van Tendeloo, S. Amelinckx, S.J. Jeng and C.M. Wayman, *J. Mat.Science*, 1986, **21**, 4395
4 B.A. Greenberg and V.I. Syutkina, New Methods for Strengthening Ordered Alloys (in Russian), Moscow: *Metallurgia*, 1985
5 B.A. Greenberg, V.I. Syutkina and E.S. Yakovleva, *Fiz. Tverdogo Tela*, 1968, **10**, 1330
6 B.A. Greenberg, O.V.Antonova, L.E. Karkina, et al., *Acta Metall. Mater.*, 1991, **39** (2), 233
7 B.A. Greenberg, N.A. Kruglikov, L.A. Rodionova, et al, *Platinum Metals Rev*, 2003, **47** (2), 46
8 A.Yu. Volkov, *Gold Bulletin*, 2004, **37** (3-4), 208
9 B.A. Greenberg, G. Hug, O.V.Antonova, et al., *Intermetallics*, 1997, **5**, 297
10 B.A. Greenberg, O.V. Antonova, A.Yu. Volkov and M.A. Ivanov, *Intermetallics*, 2000, **8**, 845
11 V. Paidar, D.P. Pope and V. Vitek, *Acta Metall*, 1984, **32** (3), 435
12 G. Hug, F. Loiseau and P. Veyssiere, *Philos. Mag. A*, 1988, **57** (3), 499
13 N.S. Stoloff and R.G. Davis, The Mechanical Properties of Ordered Alloys, Oxford: Pergamon, 1966
14 G.C. Kuczynski, R.F. Hochman and M. Doyama, *J.Appl.Phys.*, 1955, **26**, 7, 871
15 B.P. Adrianovski, V.I. Syitkina, O.D. Shashkov and A.S. Iakovleva, *The Physics of Metals and Metallography* (in Russian), 1971, **31**, 2, 392
16 D.W. Pashley, J.L. Robertson and M.J. Stowell, *Phil.Mag.*, 1969, **19**, 157, 83
17 Physical Metallurgy (Eds. R.W. Cahn and P. Haasen), 1983
18 N. Shimokawa, M. Hosomi, H. Inui, M. Yamaguchi, *Proc. Internat. Symposium Intermetallic Compounds, Sendai*, 1991, 661